

Semidilute polymer solutions at equilibrium and under shear flow

Chien-Cheng Huang¹, Roland G. Winkler^{1,*}, Godehard Sutmann², and Gerhard Gompper¹

¹*Theoretical Soft Matter and Biophysics, Institut für Festkörperforschung and Institute for Advanced Simulation, Forschungszentrum Jülich, 52425 Jülich, Germany*

²*Jülich Supercomputing Centre, Institute for Advanced Simulation, Forschungszentrum Jülich, 52425 Jülich, Germany*

(Dated: September 24, 2018)

The properties of semidilute polymer solutions are investigated at equilibrium and under shear flow by mesoscale simulations, which combine molecular dynamics simulations and the multiparticle collision dynamics approach. In semidilute solution, intermolecular hydrodynamic and excluded volume interactions become increasingly important due to the presence of polymer overlap. At equilibrium, the dependence of the radius of gyration, the structure factor, and the zero-shear viscosity on the polymer concentration is determined and found to be in good agreement with scaling predictions. In shear flow, the polymer alignment and deformation is calculated as function of concentration. Shear thinning, which is related to flow alignment and finite polymer extensibility, is characterized by the shear viscosity and the normal stress coefficients.

I. INTRODUCTION

The properties of dilute polymer solutions under shear flow have been studied intensively [1–15]. Recent advances in experimental single-molecule techniques even provide insight into the dynamics of individual polymers under shear flow [1–5, 9]. Similarly, the dynamics of individual polymers in a melt has been addressed extensively [16–21]. However, we are far from a similar understanding of the dynamics of semidilute polymer solutions, although insight into the behavior of such systems is of fundamental importance in a wide spectrum of systems ranging from biological cells, where transport appears in dense environments [22], to turbulent drag reduction in fluid flow. Moreover, in semidilute solutions of long polymers, viscoelastic effects play an important role. Due to the long structural relaxation time, the internal degrees of freedom of a polymer cannot relax sufficiently fast under non-equilibrium conditions and an elastic restoring force tries to push the system towards its original state. Here, a deeper understanding can be achieved by mesoscale hydrodynamic simulations [23, 24].

The dynamical behavior of dilute and semidilute polymer solutions is strongly affected or even dominated by hydrodynamic interactions [23–25]. From a theoretical point of view, scaling relations predicted by the Zimm model at infinite dilution, e.g., for the dependence of dynamical quantities as viscosity and relaxation time on the polymer length, are, in general, accepted and confirmed [25–27]. However, as the concentration of the polymer is increased beyond the segmental overlap concentration c^* , where the volume occupied by polymer coils is equal to the total volume, the dynamics becomes more complex due to intermolecular excluded volume interactions [25, 28–30]. For this regime, the scaling theory established by de Gennes describes the polymer dynam-

ics using the concept of 'blobs' [28]. Here a blob consists of g monomers and has the radius ξ . A polymer chain comprised of N_m monomers can be regarded as composed of N_m/g blobs which are hydrodynamically independent. Inside of a single blob, the dynamics follows the predictions of the Zimm model in dilute solution. On length scales larger than ξ , hydrodynamic and excluded volume interactions are screened due to chain overlap. Thus, the polymer dynamics on this scale can be described by the Rouse model. When the concentration is further increased, the polymer dynamics is dominated by entanglement effects, which arise from physical uncrossability of chain segments for sufficiently long polymers. Based on this theory, the relaxation time and also the zero-shear viscosity in the semidilute regime can be scaled by using the concentration ratio c/c^* , where c is the segment concentration. Various experiments confirm the predicted dependencies for the relaxation time and viscosity [29–33]. However, a systematic simulation study is still lacking, even though single-chain hydrodynamic simulations are well established [26, 27, 34–43]. The difficulty is that in the semidilute regime a large polymer overlap is necessary, whereas at the same time the segmental density has to be rather low to retain hydrodynamic interactions, which requires the simulation of long polymers [44].

The large length- and time-scale gap between the solvent and macromolecular degrees of freedom requires a mesoscale simulation approach in order to assess their structural, dynamical, and rheological properties. Here, we apply a hybrid simulation approach, combining molecular dynamics simulations (MD) for the polymers with the multiparticle collision dynamics (MPC) method describing the solvent [23, 24, 27, 45–50]. As has been shown, the MPC method is very well suited to study the non-equilibrium properties of polymers [12, 41, 51, 52], colloids [13, 53, 54], and other soft-matter object such as vesicles [55] and cells [56, 57] in flow fields.

Experiments [1–5, 9, 58], theoretical studies [11, 15], and simulations [14, 38, 40, 41, 59–62] of individual polymers under shear-flow conditions exhibit large deforma-

*Electronic address: r.winkler@fz-juelich.de

tions and a strong alignment of the polymers. Moreover, a large overlap is present in a semidilute solution of long polymers. A typical simulation requires $10^5 - 10^6$ monomers and $10^7 - 10^8$ fluid particles. Hence, despite the adopted mesoscale approach, large systems can only be studied on a massively parallel computer architecture. Here, we present results of large-scale simulations of semidilute polymer solutions under shear. The simulations were performed with our program MP²C (massively parallel multiparticle collision dynamics) [63], which exhibits excellent scaling behavior on the massively parallel architecture of the IBM Blue Gene/P computer [64]. For the MPC fluid, we find a linear increase of the speedup with increasing number of cores in a strong scaling benchmark up to 2^{12} , 2^{14} , 2^{16} cores for 10^7 , 8×10^7 , 6×10^8 fluid particles, respectively.

The paper is organized as follows. In Sec. II, the model and simulation approach are described. The equilibrium properties of the system are presented in Sec. III. Sec. IV is devoted to the structural and conformational properties of the system under stationary shear flow. In Sec. V, results are presented for the rheological properties and finally, Sec. VI summarizes our findings.

II. MODEL AND PARAMETERS

The solution consists of N_p linear flexible polymer chains embedded in an explicit solvent. A linear polymer is composed of N_m beads of mass M each, which are connected by harmonic springs. The bond potential is

$$U_b = \frac{\kappa}{2} \sum_{i=1}^{N_m-1} (|\mathbf{r}_{i+1} - \mathbf{r}_i| - l)^2, \quad (1)$$

where l is the bond length and κ the spring constant. Inter- and intramolecular excluded-volume interactions are taken into account by the repulsive, shifted, and truncated Lennard-Jones potential

$$U_{LJ} = 4\epsilon \left[\left(\frac{\sigma}{r} \right)^{12} - \left(\frac{\sigma}{r} \right)^6 + \frac{1}{4} \right] \Theta \left(2^{1/6} \sigma - r \right), \quad (2)$$

where $\Theta(x)$ is the Heaviside function [$\Theta(x) = 0$ for $x < 0$ and $\Theta(x) = 1$ for $x \geq 0$]. The dynamics of the chain monomers is determined by Newton's equations of motion, which are integrated by the velocity Verlet algorithm with the time step h_p [65].

The solvent is simulated by the multiparticle collision (MPC) dynamics method [23, 24, 45, 46]. It is composed of N_s point-like particles of mass m , which interact with each other by a stochastic process. The algorithm consists of alternating streaming and collision steps. In the streaming step, the particles move ballistically and their positions are updated according to

$$\mathbf{r}_i(t+h) = \mathbf{r}_i(t) + h\mathbf{v}_i(t), \quad (3)$$

where $i = 1, \dots, N_s$ and h is the time interval between collisions. In the collision steps, the particles are sorted

into cubic cells of side length a and their relative velocities, with respect to the center-of-mass velocity of the cell, are rotated around a randomly oriented axis by a fixed angle α , i.e.,

$$\mathbf{v}_i(t+h) = \mathbf{v}_i(t) + (\mathbf{R}(\alpha) - \mathbf{E})(\mathbf{v}_i(t) - \mathbf{v}_{cm}(t)), \quad (4)$$

where $\mathbf{v}_i(t)$ denotes the velocity of particle i at time t , $\mathbf{R}(\alpha)$ is the rotation matrix, \mathbf{E} is the unit matrix, and

$$\mathbf{v}_{cm} = \frac{1}{N_c} \sum_{j=1}^{N_c} \mathbf{v}_j, \quad (5)$$

is the center-of-mass velocity of the particles contained in the cell of particle i . N_c is the total number of solvent particles in that cell.

The solvent-polymer coupling is achieved by taking the monomers into account in the collision step, i.e., for collision cells containing monomers, the center-of-mass velocity reads

$$\mathbf{v}_{cm}(t) = \frac{\sum_{i=1}^{N_c} m\mathbf{v}_i(t) + \sum_j^{N_m} M\mathbf{v}_j(t)}{mN_c + MN_c^m}, \quad (6)$$

where N_c^m is the number of monomers within the considered collision cell. To insure Galilean invariance, a random shift is performed at every collision step [66]. The collision step is a stochastic process, where mass, momentum and energy are conserved, which leads to the build up of correlations between the particles and gives rise to hydrodynamic interactions.

To impose a shear flow, for the short chains, we apply Lees-Edwards boundary conditions [65]. A local Maxwellian thermostat is used to maintain the temperature of the fluid at the desired value [67].

A parallel MPC algorithm is exploited for systems of long chains, which is based on a three-dimensional domain-decomposition approach, where particles are sorted onto processors according to their spatial coordinates [63]. Here, shear flow is imposed by the opposite movement of two confining walls. The walls are parallel to the xy -plane and periodic boundary conditions are applied in the x - and y -directions. The equations of motion of the solvent particles are modified by the wall interaction [68]. We impose no-slip boundary conditions by the bounce-back rule, i.e., the velocity of a fluid particle is reverted when it hits a wall and phantom particles in a wall are taken into account. The same rule is applied for monomers when colliding with a wall [24].

The simulation parameters are listed in Table I. All simulation are performed with the rotation angle $\alpha = 130^\circ$. Length and time are scaled according to $\tilde{r}_\beta = r_\beta/a$, $\beta \in \{x, y, z\}$, and $\tilde{t} = t\sqrt{k_B T/(ma^2)}$, which corresponds to the choice $k_B T = 1$, $m = 1$, and $a = 1$, where T is the temperature and k_B the Boltzmann constant. The collision time is $\tilde{h} = 0.1$. The parameters yield the shear viscosity $\tilde{\eta} = \eta/\sqrt{mk_B T/a^4} = 8.7$. A large rotation angle $\alpha \gtrsim 90^\circ$ and a small time step h are advantages

to obtain high fluid viscosities, low Reynolds numbers, and larger Schmidt numbers. The selected values yield the fluid Schmidt number $Sc \approx 14$, i.e., a fluid is simulated rather than a gas [24, 49]. Between MPC collisions, the monomer dynamics is determined by molecular dynamics simulations for h/h_p steps, with $h_p = 0.002$. Moreover, we choose $l = a$, $\sigma = a$, $k_B T/\epsilon = 1$, and $\tilde{\kappa} = \kappa a^2/(k_B T) = 5 \times 10^3$. The large spring constant $\tilde{\kappa}$ ensures that the mean of the bond length changes by less than 0.5% and the variance of the bond length distribution by 3% only, even at the largest shear rate.

III. EQUILIBRIUM PROPERTIES

Before we will address polymer solutions under shear, the scaling behavior of equilibrium properties is discussed, in order to determine the crossover at which a solution starts to follow the expected scaling laws of a semidilute solution.

A. Conformational properties

The mean square radius of gyration $\langle R_{g0}^2 \rangle$ in dilute solution obeys the scaling relation

$$\langle R_{g0}^2 \rangle \propto N_m^{2\nu}, \quad (7)$$

with an exponent $\nu \approx 0.59$ for a good solvent [25, 28]. The obtained values for $\langle R_{g0}^2 \rangle$ are listed in Table I for various chain lengths. A fit of Eq. (7) to our simulation data obtained at the lowest concentrations (cf. Table 1) yields the exponent $\nu=0.61$, in good agreement with theory and experimental data [25, 28].

As the concentration increase, the polymer coils start to overlap when the monomer concentration $c = N_m N_p/V$ exceeds the value $c^* = N_m/V_p$, with the volume of a polymer $V_p = 4\pi \langle R_{g0}^2 \rangle^{3/2}/3$ and the totally available volume V [25]. Scaling considerations predict the dependence

$$\langle R_g^2 \rangle = \langle R_{g0}^2 \rangle \left(\frac{c}{c^*} \right)^{(2\nu-1)/(1-3\nu)} \quad (8)$$

for the radius of gyration at concentrations $c \gg c^*$ [25, 28]. This relation has been confirmed experimentally [69] and by computer simulations [62, 70].

Figure 1 shows radii of gyration for various polymer lengths and concentrations. Our simulation results follow the scaling predictions. For $c \ll c^*$, $\langle R_g^2 \rangle$ is independent of polymer concentration. At $c/c^* \approx 1$, the coil size starts to decrease and for $c \gg c^*$, $\langle R_g^2 \rangle \sim c^{-0.265}$ with $\nu = 0.61$.

As suggested by de Gennes, the coil overlap implies a screening of excluded volume and hydrodynamic interactions on length scales larger than the blob size ξ [25, 28]. Below this length, the swollen conformations and hydrodynamic interactions are maintained. The correlation length ξ is independent of chain length N_m and is only

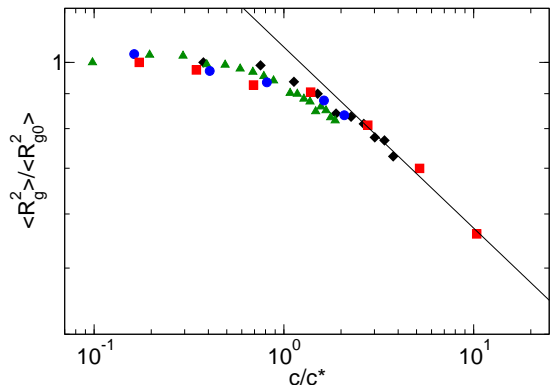


FIG. 1: Relative-mean square radii of gyration as a function of the scaled concentration c/c^* for the chain lengths $N_m = 20$ (\blacktriangle), 40 (\blacklozenge), 50 (\bullet), and 250 (\blacksquare). The solid line indicates the dependence of Eq. (8) for $\nu = 0.61$.

a function of monomer concentration at strong overlap, which yields the scaling relation

$$\xi = \langle R_{g0}^2 \rangle^{1/2} \left(\frac{c}{c^*} \right)^{-\nu/(3\nu-1)}. \quad (9)$$

The crossover is reflected in the polymer structure factor

$$S(\mathbf{q}) = \frac{1}{N_m} \sum_{i,j=1}^{N_m} \langle \exp[-i\mathbf{q}(\mathbf{r}_i - \mathbf{r}_j)] \rangle, \quad (10)$$

which exhibits the power-law dependence $S(\mathbf{q}) \sim q^{1/\delta}$ for $1 \ll q \langle R_g^2 \rangle^{1/2} \ll \langle R_g^2 \rangle^{1/2}/l$ with $\delta = 1/2$ for a melt and $\delta = \nu$ in good solvent [71]. Hence, in a semidilute solution two regimes are expected, separated by the correlation length ξ : A good solvent behavior on length scales smaller than ξ and a Gaussian chain behavior on length scales larger than ξ , i.e.,

$$S(q) \sim \begin{cases} q^{-2} & \text{for } 2\pi/\langle R_g^2 \rangle^{1/2} < q < 2\pi/\xi, \\ q^{-1/\nu} & \text{for } 2\pi/\xi < q < 2\pi/l, \end{cases} \quad (11)$$

In Fig. 2 polymer structure factors are shown for $N_m = 250$ in dilute and semidilute solutions as well as for $N_m = 50$ in dilute solution. In order to obtain the two regimes separated by ξ , the polymer chains have to be sufficiently long to provide not only a ratio $c/c^* \gg 1$ but also a low segment concentration c . As shown in the figure, for dilute solutions, $S(q)$ decays with an exponent $1/\nu$, where $\nu = 0.61$. The polymers in the semidilute regime show a crossover from the scaling behavior $S \sim q^{-2}$ at small q to the behavior $S \sim q^{-1/\nu}$ at large q values. The crossover between the two regimes corresponds to $q \approx 2\pi/\xi$. The values for ξ are presented in the inset of Fig. 2 and are found to be in excellent agreement with the scaling prediction (9) with $\nu = 0.61$. Thus, the scaling relation captures the concentration dependence of the blob size for the considered range very well.

TABLE I: List of simulation parameters. L_x, L_y, L_z denote the dimensions of the simulation box, $\dot{\gamma}$ the shear rate, and $\langle N_c \rangle$ is the mean number of fluid particles in a collision cell. For N_p, c, c^* , and $\dot{\gamma}$ the smallest and largest values used are given. Actual concentrations are provided in figure captions.

N_m	N_p	$L_x/a \times L_y/a \times L_z/a$	$\langle R_{g0}^2 \rangle / l^2$	c/l^{-3}	c^*/l^{-3}	c/c^*	$\dot{\gamma}/\sqrt{k_B T/(ma^2)}$	$\langle N_c \rangle$
20	10 – 200	20×20×20	7.05	0.025 – 0.5	0.26	0.098 – 1.96	7.5×10^{-4}	5
40	10 – 100	20×20×20	17.29	0.05 – 0.5	0.13	0.38 – 3.76	7.5×10^{-4}	5
50	10 – 512	50×50×50	24.51	0.004 – 0.205	0.098	0.041 – 2.08	$10^{-4} - 3 \times 10^{-1}$	10
250	50 – 3000	450×75×75	163.49	0.0049 – 0.296	0.029	0.17 – 10.38	$10^{-6} - 3 \times 10^{-2}$	10

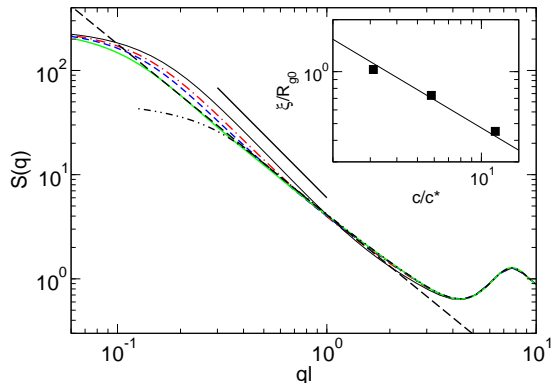


FIG. 2: Structure factors of polymers of length $N_m = 250$ for the concentration ratios $c/c^* = 0.17$ (—), $c/c^* = 2.77$ (- - -), $c/c^* = 5.19$ (- · - ·), and $c/c^* = 10.38$ (—), and of $N_m = 50$ in the dilute regime (- · · -). The dashed and solid straight lines represent power-law functions with the exponents $1/\nu = 1/0.61$ and 2, respectively. Inset: Dependence of the blob size on the concentration.

B. Dynamics

The polymer dynamics is dominated by hydrodynamic interactions in dilute solution. Theoretical results on the concentration dependence of the relaxation times for small overlap concentrations are presented in Refs. [72, 73]. Compared to the infinite-dilution limit, a term linear in the concentration is obtained, which is consistent with experimental data [30]. However, the experimental data can also well be fitted by an empirical exponential function [30].

In semidilute solution, the intermolecular interactions between different chains become increasingly important. The dynamics of the polymers can be classified according to their intermolecular interactions as unentangled or entangled [29, 30]. In the *unentangled regime*, the monomers move according to Brownian motion in all three spacial directions and their dynamics can be described by the Rouse behavior of polymers which consist of blobs. Thus, the longest relaxation time reads as

$$\tau = \tau_b \left(\frac{N_m}{g} \right)^2, \quad (12)$$

where τ_b is the blob relaxation time and g the number

of monomers in a blob. Inside of a blob, the dynamics follows the Zimm behavior

$$\tau_b \sim \left(\frac{\xi}{l} \right)^3, \quad (13)$$

and the longest relaxation time exhibits the concentration dependence

$$\tau = \tau_0 \left(\frac{c}{c^*} \right)^{(2-3\nu)/(3\nu-1)}. \quad (14)$$

In the *entangled regime*, polymers are assumed to exhibit reptation motion inside a tube caused by the presence of neighboring chains. The monomer dynamics is then described by reptation theory [28], where the longest relaxation time obeys the relation

$$\tau \sim \left(\frac{c}{c^*} \right)^{(3-3\nu)/(3\nu-1)}. \quad (15)$$

By calculating end-to-end vector correlation functions, which exhibit an exponential decay, we determined the longest polymer relaxation times τ for various concentrations. The relaxation time τ_0 at infinite dilution is obtained by extrapolation to zero concentration. The obtained values for τ_0 are shown as a function of polymer length in the inset of Fig. 3. Their length dependence is well described by the power-law $\tau_0 \sim N_m^{3\nu}$, with $\nu = 0.6$, in accord with predictions of the Zimm model [25].

Figure 3 depicts the dependence of the relaxation time on concentration. In the vicinity of $c/c^* = 1$, τ follows the scaling prediction (14) for an unentangled semidilute polymer solution. With increasing concentration, τ increases faster, which we attribute to strong intermolecular interactions. Although, there are no entanglements in our system for $c/c^* < 10$, the predicted dependence for entangled polymer melts is indicated by the solid line for illustration. This dependence is not reached and requires longer polymers or higher concentrations. A very similar dependence has been obtained experimentally in Ref. [30] over comparable concentration and relaxation time ranges.

According to the Zimm model [25, 27, 74, 75], hydrodynamic interactions strongly affect the diffusive dynamics of polymers in solution and lead to the time dependence

$$g_2(t) = \langle ([\mathbf{r}_i(t) - \mathbf{r}_{cm}(t)] - [\mathbf{r}_i(0) - \mathbf{r}_{cm}(0)])^2 \rangle \sim t^{2/3} \quad (16)$$

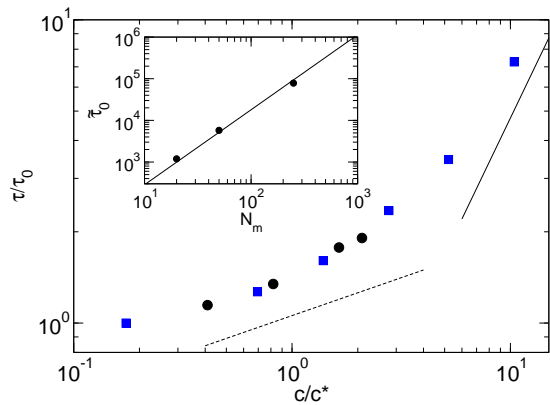


FIG. 3: Concentration dependence of longest polymer relaxation times τ for the polymer lengths $N_m = 50$ (●) and 250 (■). The dashed line indicates the prediction Eq. (14) and the continues line Eq. (15) with $\nu = 0.6$. Inset: Polymer length dependence of the relaxation time at infinite dilution. The solid line shows the dependence $\tau_0 \sim N_m^{3\nu}$ with $\nu = 0.6$.

of their monomer mean squared displacement in the center-of-mass reference frame for time scales larger than the Brownian time [76] and smaller than the longest relaxation time at which $g_2(t)$ saturates. In the semidilute regime, hydrodynamic interactions are screened for time scales larger than τ_b , the time needed to diffuse a blob diameter [44]. Consequently, after a time τ_b , the dynamics is Rouse-like and $g_2(t) \sim t^{1/2}$ [44]. Figure 4 displays $g_2(t)$ for various concentrations for polymers of length $N_m = 250$.

For a dilute solution with $c/c^* = 0.17$, $g_2(t) \sim t^{2/3}$ in the time interval $10^{-3} < t/\tau_0 < 10^{-1}$ as expected. For $t > \tau$, g_2 slowly approaches a plateau value. At larger concentrations, $g_2(t)$ displays a $t^{2/3}$ dependence which turns into a $t^{1/2}$ behavior at a time τ_b , which decrease with increasing concentration. The concentration dependence of the mean squared displacement reflects the screening of hydrodynamic interactions in the semidilute regime. However, the dependence of τ_b on concentration, which is linked to the screening length ξ_H according to $\tau_b \sim \xi_H^3$ and $\xi_H \sim c^{-\gamma}$, where γ is predicted to be 1 [77, 78], 0.6 [79], or 0.5 [28, 44], respectively, cannot be obtained unambiguously from our simulations, because the different time regimes are too short. Simulations of longer polymers are necessary to arrive at clear and pronounced diffusion regimes.

IV. SEMIDILUTE POLYMER SOLUTIONS IN SHEAR FLOW

We now discuss the properties of polymer solutions in shear flow. At infinite dilution, the flow strength is characterized by the Weissenberg number $Wi = \dot{\gamma}\tau_0$, where $\dot{\gamma}$ is the bare shear rate. For $Wi \ll 1$, the weak shear flow regime, the chains are able to undergo conforma-

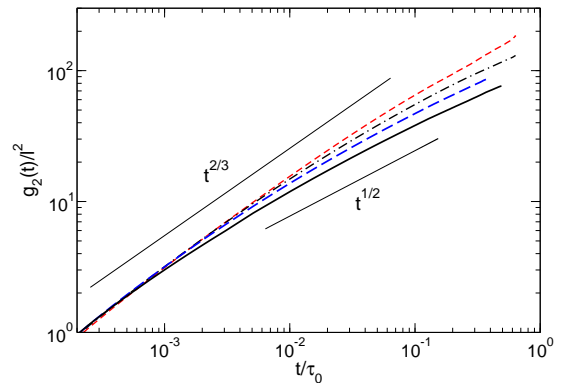


FIG. 4: Mean square displacements of monomers in the center-of-mass reference frame for the concentrations $c/c^* = 0.17$ (---), $c/c^* = 2.77$ (- · -), $c/c^* = 5.19$ (---), $c/c^* = 10.38$ (—) of polymers of length $N_m = 250$. The short lines indicate the dependencies $g_2 \sim t^{2/3}$ and $g_2 \sim t^{1/2}$, respectively.

tional changes before the local strain has changed by a detectable amount, while for $Wi \gg 1$, the chains are driven by the flow and they are not able to relax back to the equilibrium conformation. This is illustrated in figure 5, which displays snapshots for various flow rates. At small Weissenberg numbers, the polymers are only weakly perturbed and are close to their equilibrium conformations, whereas large Wi imply large deformations and a strong alignment with flow.

As pointed out in section III B, the polymer relaxation times depend on concentration. Thus, in the following, some properties will be characterized by the Weissenberg number $Wi_c = Wi\tau(c)/\tau_0 = \dot{\gamma}\tau(c)$. The question is, to what extent the influence of concentration on the polymer dynamics can be accounted for by a concentration-dependent Weissenberg number. As we will see, this concept applies well for all structural and dynamical properties.

A. Conformations

The average shape of an individual chain in solution under shear is illustrated in Fig. 6 by the density distribution of monomer positions with respect to the polymer center of mass. At low Weissenberg numbers (Fig. 6(a), (b)), the polymers are only weakly deformed and aligned with respect to the flow direction x , whereas they are considerably stretched and aligned in the flow direction and are compressed in the gradient and vorticity direction for high shear rates (Fig. 6(c), (d)). Figure 7 shows that the extent of deformation and alignment depends upon polymer concentration. At the same Weissenberg number, a larger deformation and a more pronounced alignment is found at higher concentrations.

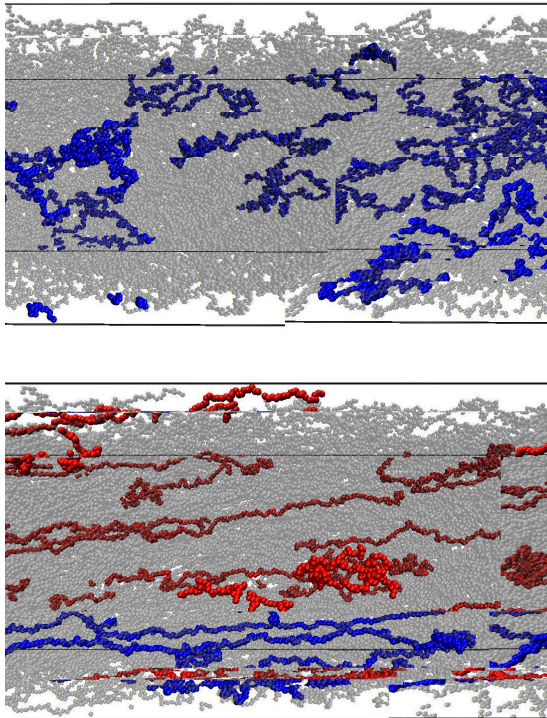


FIG. 5: Snapshots of systems with $N_p = 800$ polymers of length $N_m = 250$ for the Weissenberg numbers $Wi_c = 18$ (top) and $Wi_c = 184$ (bottom). For illustration, some of the chains are highlighted in red.

1. Radius of gyration

Polymer deformation and orientation are characterized quantitatively by the gyration tensor

$$G_{\beta\beta'} = \frac{1}{N_m} \sum_{i=1}^{N_m} \langle \Delta r_{i,\beta} \Delta r_{i,\beta'} \rangle, \quad (17)$$

where $\Delta r_{i,\beta}$ is the position of monomer i in the center-of-mass reference frame of the polymer.

In Fig. 8, the relative deformation along the flow direction

$$\delta G_{xx} = \frac{G_{xx} - G_{xx}^0}{G_{xx}^0}, \quad (18)$$

where $G_{xx}^0 = \langle R_g^2 \rangle / 3$ is the gyration tensor at equilibrium for the particular concentration, is shown for various concentrations and polymer lengths. A significant polymer stretching appears for $Wi_c > 1$. At large shear rates, the stretching saturates at a maximum, which is smaller than the value corresponding to a fully stretched chain ($G_{xx} \approx l^2 N_m^2 / 12$) and reflects the finite size of a polymer. This is consistent with experiments on DNA [2, 9], where the maximum extension is on the order of half of the contour length, and theoretical calculations [80]. It is caused by the large conformational changes of polymers in shear

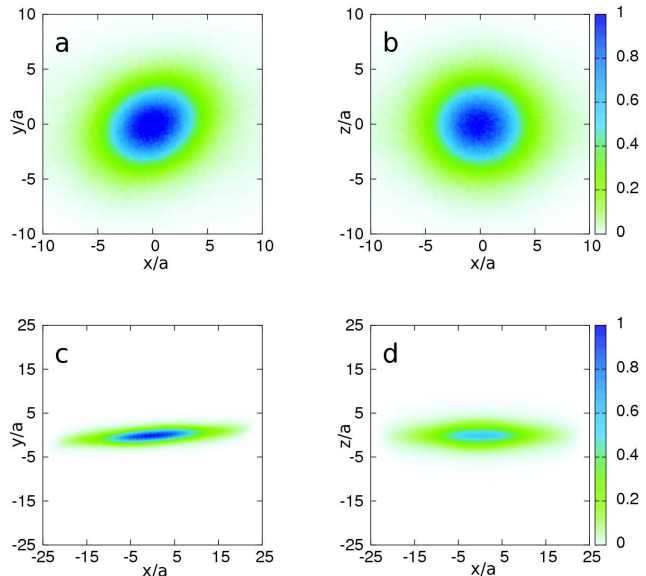


FIG. 6: Monomer density distributions in the flow-gradient plane (a), (c) and flow-vorticity plane (b), (d) for the Weissenberg numbers $Wi_c = 1$ (a), (b) and $Wi_c = 307$ (c), (d). The concentration is $c/c^* = 1.6$ and the chain length is $N_m = 50$.

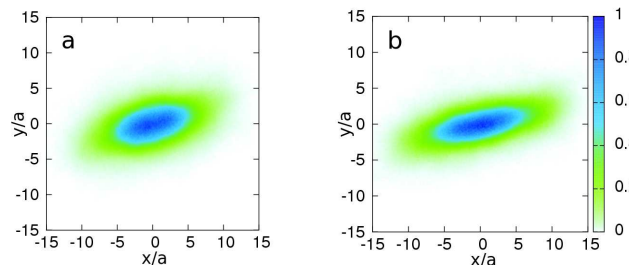


FIG. 7: Monomer density distributions in the flow-gradient plane for the shear rate $\dot{\gamma} = 10^{-3}$ and the concentrations $c/c^* = 0.16$ (a) and $c/c^* = 2.08$ (b), which corresponds to the Weissenberg numbers $Wi_c = 6.2$ and $Wi_c = 11$, respectively. The chain length is $N_m = 50$.

flow, which yields an average extension smaller than the contour length. Nevertheless, molecules assume totally stretched conformations at large Weissenberg numbers during their tumbling dynamics. Interestingly, a universal dependence is obtained for δG_{xx} as function of a concentration-dependent Weissenberg number Wi_c at a given polymer length, whereas in terms of Wi , polymers at larger concentrations exhibit a stronger stretching at the same Wi , as shown in the inset of Fig. 8 [62]. The latter is evident, since the longest relaxation time of a polymer at higher concentrations is larger and hence the polymer is more strongly deformed at the same shear

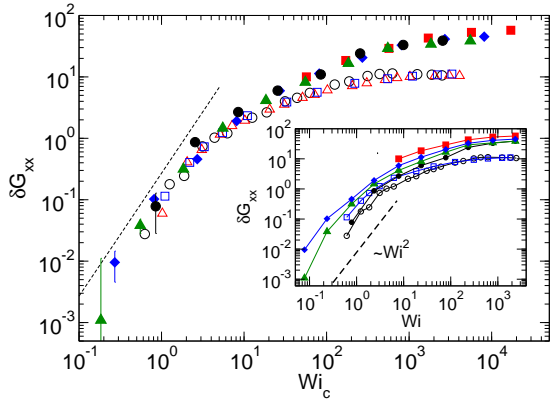


FIG. 8: Deformation ratios δG_{xx} as function of Weissenberg number. Open symbols correspond to systems with $N_m = 50$ for $c/c^* = 0.16$ (\circ), $c/c^* = 1.6$ (\triangle), and $c/c^* = 2.08$ (\square). Filled symbols denote results for $N_m = 250$ with the concentrations $c/c^* = 0.17$ (\bullet), $c/c^* = 2.77$ (\blacktriangle), $c/c^* = 5.19$ (\blacklozenge), and $c/c^* = 10.38$ (\blacksquare). In the inset, the same data are shown as function of Wi .

rate.

Theoretical calculations for single polymers in dilute solution predict the dependence $\delta G_{xx} = C_x Wi^2$ for $Wi < 1$, where C_x is a universal constant. The renormalization group calculations of Ref. [15] yield $C_x = 0.27$, whereas a calculation based on a Gaussian phantom chain model yields $C_x \approx 0.3$ [11, 60, 80–82]. As shown in Fig. 8, the simulations confirm the quadratic dependence on the shear rate; δG_{xx} is independent of chain length for $Wi < 1$ and $C_x \approx 0.1$. For $Wi > 10$, finite size effects appear and different asymptotic values are assumed for the two chain lengths. We like to stress that our simulations are in agreement with the molecular dynamics simulation results of Ref. [60] and the SANS data of Refs. [83, 84].

In the gradient and the vorticity directions, the polymers are compressed, with a smaller compression in the vorticity direction as shown in Fig. 9. To highlight the universal properties of the systems, we present the ratios $G_{\beta\beta}/G_{\beta\beta}^{00}$ ($\beta \in \{y, z\}$), where $G_{\beta\beta}^{00} = \langle R_{g0}^2 \rangle / 3$ is calculated from the radius of gyration in dilute solution at equilibrium. At low shear rates—there is no detectable shear deformation by shear—polymers shrink by concentration effects for $c/c^* > 1$ (cf. Fig. 1). This is illustrated in Fig. 9 for $Wi_c < 10$ and various concentrations. The dashed lines indicate the values of $\langle R_g^2 \rangle / \langle R_{g0}^2 \rangle$ from Fig. 1. Evidently, the ratios $G_{\beta\beta}/G_{\beta\beta}^{00}$ are consistent with the values $\langle R_g^2 \rangle / \langle R_{g0}^2 \rangle$ for each concentration. The ratio for the shorter chain $N_m = 50$ and concentration $c/c^* = 2.08$ is close to that of the longer chain with a similar concentration ratio $c/c^* = 2.77$. This is consistent with the fact that $\langle R_g^2 \rangle / \langle R_{g0}^2 \rangle$ is independent of chain length (cf. Fig. 1). With increasing shear rate, the various curves progressively approach a universal function, which decays as $\sim Wi^{-0.45}$ over the considered Wi -range. Hence, we obtain a different scaling behavior of the radius

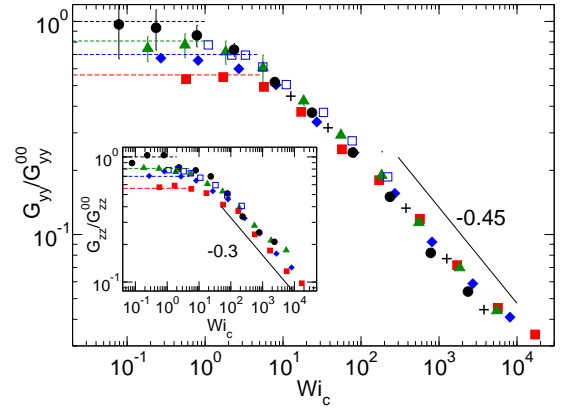


FIG. 9: Relative deformations in the gradient and vorticity direction (inset). Open symbols correspond to systems with $N_m = 50$ for $c/c^* = 2.08$ (\square). Filled symbols denote results for $N_m = 250$ with the concentrations $c/c^* = 0.17$ (\bullet), $c/c^* = 1.38$ ($+$), $c/c^* = 2.77$ (\blacktriangle), $c/c^* = 5.19$ (\blacklozenge), and $c/c^* = 10.38$ (\blacksquare).

of gyration along the flow direction and the transverse directions. The reason is that a high monomer density is maintained along the flow direction due to polymer stretching, whereas the density in the transverse directions decreases by flow-induced polymer shrinkage.

The exponents of the power-law decay of G_{yy} and G_{zz} compare well with the experimental data on single DNA molecules [9]. Similarly, simulations (with/without hydrodynamic and excluded volume interactions) yield comparable exponents [9, 85]. However, simulations in Ref. [9] for even larger Weissenberg numbers seem to produce an exponent closer to the theoretically expected value of $2/3$ [11, 80]. According to theory, there is a broad crossover regime before the asymptotic behavior at large Weissenberg numbers is assumed, and the considered Wi fall into that crossover regime.

2. Alignment

The alignment of the polymers is characterized by the angle χ_G , which is the angle between the eigenvector of the gyration tensor with the largest eigenvalue and the flow direction. It is obtained from the components of the radius of gyration tensor via [14]

$$\tan(2\chi_G) = \frac{2G_{xy}}{G_{xx} - G_{yy}}. \quad (19)$$

The dependence of $\tan(2\chi_G)$ on shear rate and concentration is shown in Fig. 10. Again, a universal curve is obtained for the different concentrations at a given polymer length. Moreover, $\tan(2\chi_G)$ seems to be independent of polymer length for $Wi_c < 100$, whereas we find a length dependence for larger Weissenberg numbers. In this high

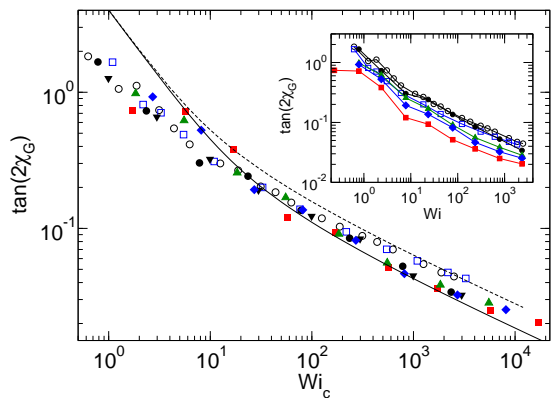


FIG. 10: Dependence of $\tan(2\chi_G)$ on shear rate. Open symbols correspond to systems with $N_m = 50$ for $c/c^* = 0.16$ (\circ) and $c/c^* = 2.08$ (\square). Filled symbols denote results for $N_m = 250$ with the concentrations $c/c^* = 0.17$ (\bullet), $c/c^* = 0.35$ (\blacktriangleleft), $c/c^* = 0.69$ (\blacktriangledown), $c/c^* = 2.77$ (\blacktriangle), $c/c^* = 5.19$ (\blacklozenge), and $c/c^* = 10.38$ (\blacksquare). The solid and dashed lines are theoretical results [11, 80]. In the inset, the same data are shown as function of Wi . Lines are guides for the eye only.

shear rate regime, we find $\tan(2\chi_G) \sim (Wi_c)^{-1/3}$. We like to emphasize that only the shear rate can be scaled in order to arrive at a universal function. The angle, or $\tan(2\chi_G)$, cannot be scaled to absorb flow or polymer properties in an effective variable. Hence, the universal behavior of the alignment angle for various concentrations confirms that the Weissenberg number Wi_c is the correct scaling variable and that the alignment of polymers at different concentrations depends on the combination $Wi_c = \dot{\gamma}\tau$ of shear rate and relaxation time only.

The analytical description of Refs. [11, 80] predicts the dependence

$$\tan(2\chi_G) \sim \left(\frac{l_p}{LWi^*} \right)^{1/3} \quad (20)$$

for semiflexible polymers in dilute solution in the limit $Wi^* \rightarrow \infty$. Here, we introduce the Weissenberg number $Wi^* = \dot{\gamma}\tau_{th}$ for the theoretical result, because the relaxation times from theory and simulation might not be the same; L is the length and l_p the persistence length of the polymer. The analytical result describes the simulation data well at large shear rates, when the Weissenberg number of the theoretical model is set to $Wi^* = Wi_c/2$. To compare the predicted length dependence with that of the simulation, we apply the relation $\langle R_{e0}^2 \rangle = 2l_pL$ to obtain a persistence length, with $\langle R_{e0}^2 \rangle$ the polymer mean square end-to-end distance in dilute solution at equilibrium, which yields $l_p/L \approx 0.025$ for $N_m = 50$ and $l_p/L \approx 0.008$ for $N_m = 250$. With these values, the ratio of $\tan(2\chi_G)$ of the polymer of length $L = 50a$ and $L = 250a$ is 1.5. This compares well with the factor 1.33 following from the simulation results, which suggests that excluded volume interactions are of minor importance for intermediate flow rates.

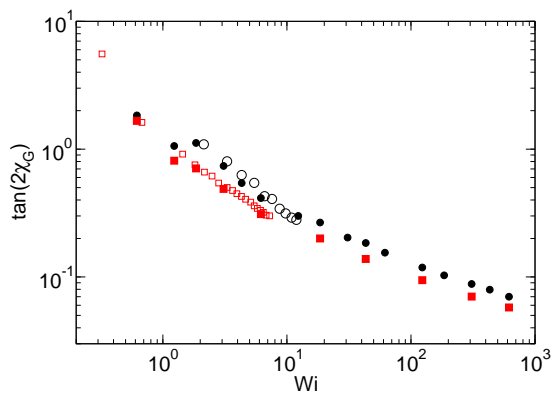


FIG. 11: Comparison of experimental and simulation data for the average orientation angle χ_G . The concentrations are $c = 0.016/l^{-3}$ (\bullet), $c = 0.205/l^{-3}$ (\blacksquare) for our simulations (with $N_m = 50$), and $0.113g/l$ (\circ), $1.094g/l$ (\square) for the experiments [86].

In the limit $Wi_c \rightarrow 0$, theory predicts $\tan(2\chi_G) \sim Wi_c^{-1}$. The simulation data do not show this dependence on the considered range of Weissenberg numbers, which might be due to excluded volume interactions.

The inset of Fig. 10 displays a strong dependence of χ_G on concentration. The higher the concentration, the more the chains are orientated along the flow direction. Such a concentration effect has also been reported in light scattering experiments [86], where dilute polymer solutions are considered. A comparison of the experimental data with the simulation results is presented in Fig. 11. Two data sets are presented, a dilute solution, with the concentration $0.113g/l$, and a semidilute solution with the approximately ten times higher concentration $1.094g/l$, both taken from Fig. 8 of Ref. [86]. Evidently, the experimental data fit well with our simulation results. Moreover, both, experiments and simulations, yield a shift of the curves for the higher concentrations to smaller Weissenberg numbers. In Ref. [86], a factor $\beta_e \sim [\eta]\dot{\gamma}$, where $[\eta]$ is the intrinsic viscosity, is used to present the data. This quantity is proportional to Wi , since $[\eta]$ is proportional to the longest relaxation time τ ; however, β_e and Wi are not identical. No adjustment parameter is used in Fig. 11, which suggests that the ratio β_e/Wi is close to unity.

V. RHEOLOGY

A. Shear viscosity

Under shear flow, the viscosity $\eta(\dot{\gamma})$ is obtained from the relation

$$\eta(\dot{\gamma}) = \frac{\sigma_{xy}(\dot{\gamma})}{\dot{\gamma}}, \quad (21)$$

where σ_{xy} is the shear stress [87, 88]. In our simulations, σ_{xy} is calculated using the virial formulation of the stress tensor [65, 68, 89]. For sufficiently weak flow, the polymer solution is in the Newtonian regime, i.e., $\sigma_{xy} \sim \dot{\gamma}$ and the viscosity is independent of shear rate. Thus, the viscosity obtained in this low shear rate regime is equal to the zero-shear viscosity denoted by η_0 . The latter depends on the monomer concentration, which is often presented in the form

$$\eta_0 = \eta_s [1 + [\eta]c + k_H([\eta]c)^2 + \dots], \quad (22)$$

where η_s is the solvent viscosity and k_H the Huggins constant [31, 87].

We determine the intrinsic viscosity by a linear extrapolation to zero concentration of both, $(\eta_0 - \eta_s)/c\eta_s$ and the inherent specific viscosity $[\ln(\eta_0/\eta_s)]/c$. The common intercept of these two functions gives $[\eta]$ [31, 90].

The intrinsic viscosity is proportional to R_g^3/N_m [25] and is therefore proportional to the inverse of the overlap concentration c^* [29, 91]. We find $[\eta]c^* \approx 0.9$ and $[\eta]c^* \approx 1$ for the polymer of length $N_m = 40$ and $N_m = 50$, respectively, which means that the proportionality coefficient is close to unity for the considered model systems.

The Einstein relation

$$\eta = \eta_s (1 + 2.5\phi), \quad (23)$$

where ϕ is the volume fraction, captures the concentration dependence of hard sphere suspensions for $\phi \ll 1$. This relation should also apply for dilute polymer solutions, when the hydrodynamic radius R_H is used to define the volume fraction, i.e., $\phi = (4\pi/3)R_H^3 N_p/V$. Equations (22) and (23) are consistent if $[\eta]c^* = 2.5(R_H/R_g)^3$. Since $[\eta]c^* \approx 1$, as explained above, consistency requires $R_g/R_H \approx 1.36$. From our simulations, we find the hydrodynamic radii $R_H \approx 3.8l$ and $R_H \approx 9.4l$ for the polymers of length $N_m = 50$ and $N_m = 250$, respectively, which yields the ratios 1.3 and 1.36. These values are very close to the value necessary to match the Einstein relation. The ratios are somewhat smaller than the asymptotic value $R_g/R_H \approx 1.59$ for $N_m \rightarrow \infty$ obtained in Ref. [82], which is a consequence of the fact that we consider insufficiently long chains.

The term $k_H([\eta]c)^2$ depends on hydrodynamic interactions. The value of the Huggins constant k_H of flexible polymers is in the range of 0.2 – 0.8 and depends on solvent quality [31, 90]. In good solvent, typically the value 0.3 is found experimentally [90]. Expressing Eq. (22) in terms of the dimensionless parameter $[\eta]c$ as

$$\eta_R = \frac{(\eta_0 - \eta_s)}{\eta_s [\eta]c} = 1 + k_H [\eta]c + \dots, \quad (24)$$

which is denoted as relative viscosity, allows us to determine k_H . The inset of Fig. 12 shows $\eta_R - 1$ as function of $[\eta]c$ for polymers of length $N_m = 40$ and $N_m = 50$. The slope of the solid line is $k_H = 0.35$, in close agreement with experiments [31, 90].

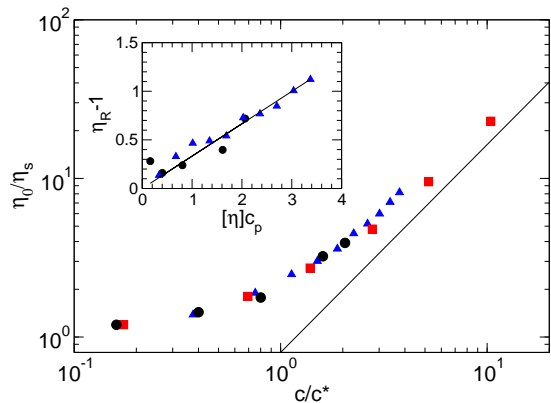


FIG. 12: Dependence of the zero shear viscosity on the scaled concentration c/c^* for the polymer lengths $N_m = 40$ (\blacktriangle), $N_m = 50$ (\bullet), and $N_m = 250$ (\blacksquare). The solid line indicates the power-law $(c/c^*)^{1/(3\nu-1)}$ with $\nu = 0.6$. In the inset, $\eta_R - 1$, Eq (24), is shown as function of $[\eta]c$ for $N_m = 40$ (\blacktriangle) and $N_m = 50$ (\bullet); the slope of the solid line is 0.35, which corresponds to the Huggins constant of polymers in good solvent.

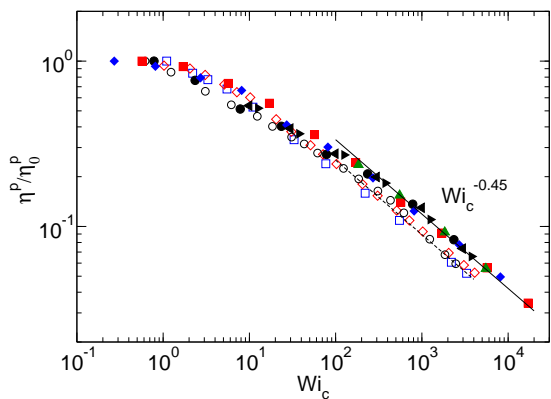


FIG. 13: Dependence of the polymer contribution to shear viscosity on shear rate. Open symbols correspond to systems with $N_m = 50$ for $c/c^* = 0.16$ (\circ), $c/c^* = 1.6$ (\diamond), and $c/c^* = 2.08$ (\square). Filled symbols denote results for $N_m = 250$ with the concentration $c/c^* = 0.17$ (\bullet), $c/c^* = 0.35$ (\blacktriangleleft), $c/c^* = 1.38$ (\blacktriangleright), $c/c^* = 2.77$ (\blacktriangle), $c/c^* = 5.19$ (\blacklozenge), and $c/c^* = 10.38$ (\blacksquare).

For semidilute unentangled polymer solutions, the viscosity is proportional to the number of blobs per chain and can be expressed by the scaling relation [28, 29, 31, 33]

$$\eta_0 = \eta_s \left(\frac{c}{c^*} \right)^{1/(3\nu-1)}. \quad (25)$$

Figure 12 displays zero-shear viscosities as function of concentration for various polymer lengths. For $c/c^* \gtrsim 3$, the data are close to the power-law of Eq. (25).

At sufficiently large shear rates, the polymers are aligned and deformed, which implies shear thinning [11, 14, 80, 88]. Figure 13 shows the polymer contribution

η^p to the shear viscosity. Similar to the alignment angle, the viscosity is a universal function of the Weissenberg number Wi_c and shows a weak dependence on polymer length. It is independent of shear rate for $Wi_c \ll 1$, decrease approximately as $Wi_c^{-0.3}$ for $1 < Wi_c < 10^2$, and $Wi_c^{-0.45}$ for higher shear rates. This behavior is consistent with other simulation results [9, 38, 40, 59, 92]. However, an even stronger decay of the viscosity is observed in simulations at larger shear rates in Refs. [9, 14]. Experiments of dilute polymer solutions reported exponents ranging from -0.4 to -0.85 [9, 88]. Theoretical calculations for dumbbells and finite extendable polymers predict the dependence $\eta_p \sim Wi^{-2/3}$ in the limit $Wi \rightarrow \infty$ [11, 18, 80, 88, 93]. The differences in the observed behavior can be explained by a broad crossover regime before the asymptotic behavior is reached.

The ratio of the viscosities of the two lengths is approximately 1.33 for the large Weissenberg-number regime, as for the alignment angle, which compares well with the theoretically predicted length dependence in Eq. (20) (cf. Sec. IV A. 2).

B. Normal stress coefficient

The concentration and shear rate dependencies of the first and second normal stress difference [88, 93]

$$\Psi_1 = (\sigma_{xx} - \sigma_{yy}) / \dot{\gamma}^2, \quad (26)$$

$$\Psi_2 = (\sigma_{yy} - \sigma_{zz}) / \dot{\gamma}^2 \quad (27)$$

are displayed in Fig. 14. Within the accuracy of the simulations, the ratio Ψ_1 / Ψ_1^0 , where Ψ_1^0 is the stress difference at zero shear rate, is an universal function of Wi_c for various concentrations and decreases as $\Psi_1 \sim \dot{\gamma}^{-4/3}$ for large shear rates. This is consistent with analytical calculations [80, 88, 93], various computer simulations [9, 38, 40, 59, 93, 94], and experiments [2, 3] for dilute solutions. Similar to the viscosity, the decrease is related to the finite polymer extensibility. Both, hydrodynamic and excluded volume interactions contribute to Ψ_1 , which is shown in Ref. [38] for single polymers. Here, we find the power law

$$\Psi_1^0 \sim \left(\frac{c}{c^*}\right)^{1.3}, \quad (28)$$

as shown in the inset of Fig. 14(a). Hence, the first normal stress difference exhibits a significant dependence on excluded volume interactions. At large concentrations, Ψ_1^0 might saturate; at least, we cannot exclude such a saturation at the upper limit of the considered concentration range.

Second normal stress differences are presented in Fig. 14(b) for various concentrations. At low concentrations, their values are much smaller than those of Ψ_1 , and hence cannot be calculated within the same accuracy, and the values Ψ_2^0 are difficult to find. We therefore present the simulations results for Ψ_2 directly rather than

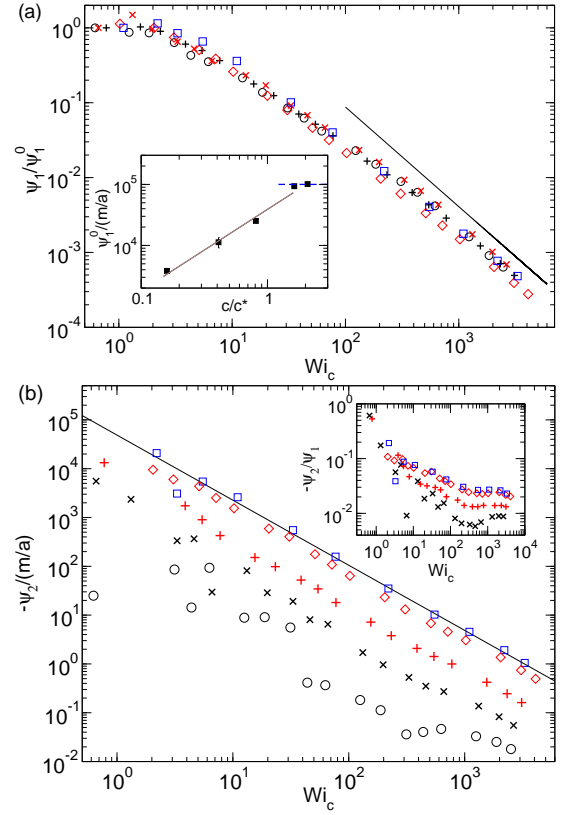


FIG. 14: First and second normal stress coefficients Ψ_1 (a) and Ψ_2 (b) for polymers of length $N_m = 50$ and the concentrations $c/c^* = 0.16$ (\circ), $c/c^* = 0.41$ (\times), $c/c^* = 0.81$ ($+$), $c/c^* = 1.63$ (\diamond) and $c/c^* = 2.08$ (\square). The solid lines indicate the power-law decay $\Psi_i \sim Wi_c^{-4/3}$. Inset in (a): Concentration dependence of the zero-shear-rate first normal stress coefficient Ψ_1^0 . Inset in (b): Ratio of Ψ_2/Ψ_1 for the various concentrations.

in scaled form. Similar to Ψ_1 , the second normal stress difference decreases as $\Psi_2 \sim \dot{\gamma}^{-4/3}$ with increasing shear rate. Again, excluded volume and hydrodynamic interactions contribute to Ψ_2 [38, 88, 93]. The ratio Ψ_2/Ψ_1 is concentration dependent, as shown in Fig. 14(b). At small Wi_c and large concentrations, the ratio is close to unity, decreases with increasing shear rate and assumes a constant value above a certain Wi_c , which seems to depend on concentration. The plateau value itself increases with increasing concentration. A similar plateau has been found in simulations of dilute solutions in Ref. [40]. The concentration dependence of the plateau value suggests that excluded volume interactions determine the behavior of the normal stress differences. If hydrodynamic interactions would be dominant, we would expect a decrease of the plateau with increasing concentration due to screening of hydrodynamic interactions by polymer overlap.

VI. CONCLUSIONS

We have calculated conformational, dynamical, and rheological properties of polymers in dilute and semidilute solution under shear flow by mesoscale hydrodynamic simulations. At equilibrium, our simulations confirm the scaling predictions for the concentration dependence of the radius of gyration and the longest relaxation time. Moreover, we find signatures for the screening of excluded volume interactions in the static structure factor.

In shear flow, the polymers exhibit deformation—the polymer is stretched in flow direction and shrinks in the transverse directions—and alignment, which depend on shear rate and concentration. As one of the main results of the paper, we have shown that the relative deformation δG_{xx} in the flow direction, the alignment $\tan(2\chi_G)$, and the viscosity η/η_0 are universal functions of the concentration-dependent Weissenberg number $Wi_c = \dot{\gamma}\tau(c)$ [92, 95]. This is surprising because τ increases rapidly with increasing concentration. Moreover, it indicates that the dynamics under shear flow is still governed by the relaxation time at equilibrium despite the anisotropic deformation of a polymer. This is not evident a priori, as expressed by the scaling behavior of the radius of gyration tensor components G_{yy} and G_{zz} . Here, we find a concentration-independent scaling behavior at large Wi_c only when these values are scaled

by their equilibrium values in *dilute solution*. Hence, the deformations transverse to the flow directions seem to exhibit a scaling behavior corresponding to a dilute solution, however, with the relaxation time of the concentrated system.

In addition, the zero-shear viscosity obeys the scaling predictions with respect to the concentration dependence. Moreover, for the first time, we show by simulations that the Huggins constant is equal to $k_H = 0.35$ for a flexible polymer in good solvent, which is in close agreement with experimental results [90].

Finally, we find a strong concentration dependence of the normal stress differences. Their ratio shows that intermolecular excluded volume interactions determine their behavior at all shear rates.

Our simulations reveal a complex interplay between shear rate, deformation, and intramolecular excluded volume interactions, which is difficult to grasp by analytical theory.

Acknowledgments

The financial support by the Deutsche Forschungsgemeinschaft (DFG) within SFB TR6 (project A4) is gratefully acknowledged. We are grateful to the Jülich Supercomputer Centre (JSC) for allocation of a special CPU-time grant.

-
- [1] D. E. Smith, H. P. Babcock, and S. Chu, *Science* **283**, 1724 (1999).
 - [2] C. M. Schroeder, R. E. Teixeira, E. S. G. Shaqfeh, and S. Chu, *Phys. Rev. Lett.* **95**, 018301 (2005).
 - [3] R. E. Teixeira, H. P. Babcock, E. S. G. Shaqfeh, and S. Chu, *Macromolecules* **38**, 581 (2005).
 - [4] S. Gerashchenko and V. Steinberg, *Phys. Rev. Lett.* **96**, 038304 (2006).
 - [5] P. S. Doyle, B. Ladoux, and J.-L. Viovy, *Phys. Rev. Lett.* **84**, 4769 (2000).
 - [6] A. Celani, A. Puliafito, and K. Turitsyn, *Europhys. Lett.* **70**, 464 (2005).
 - [7] M. Chertkov, I. Kolokolov, A. Lebedev, and K. Turitsyn, *J. Fluid. Mech.* **531**, 251 (2005).
 - [8] A. Puliafito and K. Turitsyn, *Physica D* **211**, 9 (2005).
 - [9] C. M. Schroeder, R. E. Teixeira, E. S. G. Shaqfeh, and S. Chu, *Macromolecules* **38**, 1967 (2005).
 - [10] R. Delgado-Buscalioni, *Phys. Rev. Lett.* **96**, 088303 (2006).
 - [11] R. G. Winkler, *Phys. Rev. Lett.* **97**, 128301 (2006).
 - [12] R. G. Winkler, K. Mussawisade, M. Ripoll, and G. Gompper, *J. Phys.: Condens. Matter* **16**, S3941 (2004).
 - [13] M. Ripoll, R. G. Winkler, and G. Gompper, *Phys. Rev. Lett.* **96**, 188302 (2006).
 - [14] C. Aust, M. Kröger, and S. Hess, *Macromolecules* **32**, 5660 (1999).
 - [15] S. Q. Wang, *J. Chem. Phys.* **92**, 7618 (1990).
 - [16] T. C. B. McLeish, *Adv. Phys.* **51**, 1379 (2002).
 - [17] M. Kröger, *Phys. Rep.* **390**, 453 (2004).
 - [18] M. Rubinstein and R. Colby, *Polymer Physics* (Oxford University Press, Oxford, 2003).
 - [19] J. M. Kim, B. J. Edwards, D. J. Keffer, and B. Khomami, *Phys. Lett. A* **373**, 769 (2009).
 - [20] P. P. Jose and G. Szamel, *J. Chem. Phys.* **127**, 114095 (2007).
 - [21] P. P. Jose and G. Szamel, *J. Chem. Phys.* **128**, 224910 (2008).
 - [22] R. Ellis and A. Minton, *Nature* **425**, 27 (2003).
 - [23] R. Kapral, *Adv. Chem. Phys.* **140**, 89 (2008).
 - [24] G. Gompper, T. Ihle, D. M. Kroll, and R. G. Winkler, *Adv. Polym. Sci.* **221**, 1 (2009).
 - [25] M. Doi and S. F. Edwards, *The Theory of Polymer Dynamics* (Clarendon Press, Oxford, 1986).
 - [26] P. Ahlrichs and B. Dünweg, *J. Chem. Phys.* **111**, 8225 (1999).
 - [27] K. Mussawisade, M. Ripoll, R. G. Winkler, and G. Gompper, *J. Chem. Phys.* **123**, 144905 (2005).
 - [28] P.-G. de Gennes, *Scaling Concepts in Polymer Physics* (Cornell University, Ithaca, 1979).
 - [29] E. Raspaud, D. Lairez, and M. Adam, *Macromolecules* **28**, 927 (1995).
 - [30] S. S. Patel and K. M. Takahashi, *Macromolecules* **25**, 4382 (1992).
 - [31] Y. Takahashi, Y. Isono, I. Noda, and M. Nagasawa, *Macromolecules* **18**, 1002 (1985).
 - [32] M. Adam and M. Delsanti, *J. Physique* **44**, 1185 (1983).
 - [33] Y. Heo and R. G. Larson, *J. Rheol.* **49**, 1117 (2005).

- [34] C. Pierleoni and J.-P. Ryckaert, Phys. Rev. Lett **66**, 2992 (1991).
- [35] B. Dünweg and K. Kremer, Phys. Rev. Lett **66**, 2996 (1991).
- [36] C. Pierleoni and J.-P. Ryckaert, J. Chem. Phys. **96**, 8539 (1992).
- [37] A. V. Lyulin, D. B. Adolf, and G. R. Davies, J. Chem. Phys. **111**, 758 (1999).
- [38] D. Petera and M. Muthukumar, J. Chem. Phys. **111**, 7614 (1999).
- [39] R. M. Jendrejack, J. J. de Pablo, and M. D. Graham, J. Chem. Phys. **116**, 7752 (2002).
- [40] C.-C. Hsieh and R. G. Larson, J. Rheol. **48**, 995 (2004).
- [41] J. F. Ryder and J. M. Yeomans, J. Chem. Phys. **125**, 194906 (2006).
- [42] C. Sendner and R. R. Netz, EPL **81**, 54006 (2007).
- [43] Y. Zhang, A. Donev, T. Weisgraber, B. J. Alder, M. G. Graham, and J. J. de Pablo, J. Chem. Phys. **130**, 234902 (2009).
- [44] P. Ahlrichs, R. Everaers, and B. Dünweg, Phys. Rev. E **64**, 040501(R) (2001).
- [45] A. Malevanets and R. Kapral, J. Chem. Phys. **110**, 8605 (1999).
- [46] A. Malevanets and R. Kapral, J. Chem. Phys. **112**, 7260 (2000).
- [47] A. Malevanets and J. M. Yeomans, Europhys. Lett. **52**, 231 (2000).
- [48] M. Ripoll, K. Mussawisade, R. G. Winkler, and G. Gompper, Europhys. Lett. **68**, 106 (2004).
- [49] M. Ripoll, K. Mussawisade, R. G. Winkler, and G. Gompper, Phys. Rev. E **72**, 016701 (2005).
- [50] J. T. Padding and A. A. Louis, Phys. Rev. E **73**, 031402 (2006).
- [51] L. Cannavacciuolo, R. G. Winkler, and G. Gompper, EPL **83**, 34007 (2008).
- [52] R. Chelakkot, R. G. Winkler, and G. Gompper, EPL **91**, 14001 (2010).
- [53] J. T. Padding and A. A. Louis, Phys. Rev. Lett. **93**, 220601 (2004).
- [54] A. Wysocki, C. P. Royall, R. G. Winkler, G. Gompper, H. Tanaka, A. van Blaaderen, and H. Löwen, Soft Matter **5**, 1340 (2009).
- [55] H. Noguchi and G. Gompper, Phys. Rev. Lett. **93**, 258102 (2004).
- [56] H. Noguchi and G. Gompper, Proc. Natl. Acad. Sci. USA **102**, 14159 (2005).
- [57] J. L. McWhirter, H. Noguchi, and G. Gompper, Proc. Natl. Acad. Sci. USA **106**, 6039 (2009).
- [58] P. LeDuc, C. Haber, G. Boa, and D. Wirtz, Nature **399**, 564 (1999).
- [59] T. W. Liu, J. Chem. Phys. **90**, 5826 (1989).
- [60] C. Pierleoni and J.-P. Ryckaert, Macromolecules **28**, 5097 (1995).
- [61] C. Pierleoni and J.-P. Ryckaert, J. Chem. Phys. **113**, 5545 (2000).
- [62] C. Stoltz, J. J. de Pablo, and M. D. Graham, J. Rheol. **50**, 137 (2005).
- [63] G. Sutmman, C.-C. Huang, R. G. Winkler, and G. Gompper, in *John von Neumann Institute for Computing NIC Symposium 2010*, edited by G. Münster, D. Wolf, and M. Kremer (Forschungszentrum Jülich, Jülich, 2010), vol. 3 of *IAS Series*, pp. 287–294.
- [64] G. Sutmman, R. G. Winkler, and G. Gompper, unpublished.
- [65] M. P. Allen and D. J. Tildesley, *Computer Simulation of Liquids* (Clarendon Press, Oxford, 1987).
- [66] T. Ihle and D. M. Kroll, Phys. Rev. E **63**, 020201(R) (2001).
- [67] C.-C. Huang, A. Chatterji, G. Sutmman, G. Gompper, and R. G. Winkler, J. Comput. Phys. **229**, 168 (2010).
- [68] R. G. Winkler and C.-C. Huang, J. Chem. Phys. **130**, 074907 (2009).
- [69] M. Daoud, J. P. Cotton, B. Farnoux, G. Jannink, G. Sarma, C. D. H. Benoit, C. Picot, and P. G. de Gennes, Macromolecules **8**, 804 (1975).
- [70] A. Pelissetto, J. Chem. Phys. **129**, 044901 (2008).
- [71] G. Strobel, *The Physics of Polymers* (Springer, Berlin, 2007).
- [72] M. Muthukumar and K. F. Freed, Macromolecules **11**, 843 (1978).
- [73] M. Muthukumar, Macromolecules **17**, 971 (1984).
- [74] B. H. Zimm, J. Chem. Phys. **24**, 269 (1956).
- [75] L. Harnau, R. G. Winkler, and P. Reineker, J. Chem. Phys. **104**, 6355 (1996).
- [76] J. K. G. Dhont, *An Introduction to Dynamics of Colloids* (Elsevier, Amsterdam, 1996).
- [77] K. F. Freed and S. F. Edwards, J. Chem. Phys. **64**, 1290 (1974).
- [78] S. F. Edwards and M. Muthukumar, Macromolecules **17**, 586 (1984).
- [79] G. H. Frederickson and E. Helfand, J. Chem. Phys. **93**, 2048 (1990).
- [80] R. G. Winkler, J. Chem. Phys. (2010), accepted for publication.
- [81] W. Bruns and W. Carl, Macromolecules **26**, 557 (1993).
- [82] W. Carl and W. Bruns, Macromol. Theory Simul. **3**, 295 (1994).
- [83] P. Lindner and R. C. Oberthur, Colloid Polym. Sci. **266**, 886 (1988).
- [84] P. Lindner and R. C. Oberthur, Physica B **156 & 157**, 410 (1989).
- [85] J. S. Hur, E. S. G. Shaqfeh, and R. G. Larson, J. Rheol. **44**, 713 (2000).
- [86] A. Link and J. Springer, Macromolecules **26**, 464 (1993).
- [87] R. B. Bird, R. C. Armstrong, and O. Hassager, *Dynamics of Polymeric Liquids*, vol. 1 (Wiley, New York, 1976).
- [88] R. B. Bird, O. Hassager, R. C. Armstrong, and C. F. Curtiss, *Dynamics of Polymeric Liquids*, vol. 2 (John Wiley Sons, New York, 1987).
- [89] R. G. Winkler, M. Morawitz, and D. Y. Yoon, Mol. Phys. **75**, 669 (1992).
- [90] R. Pamies, J. G. H. Cifre, and M. del Carmen Lopez Martinez, Colloid Polym. Sc. **286**, 1223 (2008).
- [91] G. Weill and J. des Cloizeaux, J. Phys. France **40**, 99 (1979).
- [92] A. Galuschko, L. Spirin, T. Kreer, A. Johner, C. Pastorino, J. Wittmer, and J. Baschnagel, Langmuir **26**, 6418 (2010).
- [93] H. C. Öttinger, *Stochastic Processes in Polymeric Fluids* (Springer, Berlin, 1996).
- [94] W. Zylka, J. Chem. Phys. **94**, 4628 (1991).
- [95] J. Hur, E. S. G. Shaqfeh, H. P. Babcock, D. E. Smith, and S. Chu, J. Rheol. **45**, 421 (2001).